

## Article

# Palmitic Acid-Conjugated Radiopharmaceutical for Integrin $\alpha_v\beta_3$ -Targeted Radionuclide Therapy

Guangjie Yang<sup>1</sup>, Hannan Gao<sup>2</sup>, Chuangwei Luo<sup>1</sup>, Xiaoyu Zhao<sup>1</sup>, Qi Luo<sup>3</sup>, Jiyun Shi<sup>2,\*</sup>  and Fan Wang<sup>1,2,3,\*</sup> 

<sup>1</sup> Medical Isotopes Research Center and Department of Radiation Medicine, State Key Laboratory of Natural and Biomimetic Drugs, School of Basic Medical Sciences, Peking University, Beijing 100191, China; docyang@bjmu.edu.cn (G.Y.); luocw@bjmu.edu.cn (C.L.); 2011110025@bjmu.edu.cn (X.Z.)

<sup>2</sup> Key Laboratory of Protein and Peptide Pharmaceuticals, CAS Center for Excellence in Biomacromolecules, Institute of Biophysics, Chinese Academy of Sciences, Beijing 100101, China; gaohannan@ibp.ac.cn

<sup>3</sup> Guangzhou Laboratory, Guangzhou 510005, China; luo\_qi@gzlab.ac.cn

\* Correspondence: shijiyun@ibp.ac.cn (J.S.); wangfan@bjmu.edu.cn (F.W.)

**Abstract:** Peptide receptor radionuclide therapy (PRRT) is an emerging approach for patients with unresectable or metastatic tumors. Our previously optimized RGD peptide (3PRGD<sub>2</sub>) has excellent targeting specificity for a variety of integrin  $\alpha_v\beta_3/\alpha_v\beta_5$ -positive tumors and has been labeled with the therapeutic radionuclide [<sup>177</sup>Lu]LuCl<sub>3</sub> for targeted radiotherapy of tumors. However, the rapid clearance of [<sup>177</sup>Lu]Lu-DOTA-3PRGD<sub>2</sub> (<sup>177</sup>Lu-3PRGD<sub>2</sub>) in vivo requires two doses of 111 MBq/3 mCi to achieve effective tumor suppression, limiting its further clinical application. Albumin binders have been attached to drugs to facilitate binding to albumin in vivo to prolong the drug half-life in plasma and obtain long-term effects. In this study, we modified 3PRGD<sub>2</sub> with albumin-binding palmitic acid (Palm-3PRGD<sub>2</sub>) and then radiolabeled Palm-3PRGD<sub>2</sub> with <sup>177</sup>Lu. [<sup>177</sup>Lu]Lu-DOTA-Palm-3PRGD<sub>2</sub> (<sup>177</sup>Lu-Palm-3PRGD<sub>2</sub>) retained a specific binding affinity for integrin  $\alpha_v\beta_3/\alpha_v\beta_5$ , with an IC<sub>50</sub> value of 5.13 ± 1.16 nM. Compared with <sup>177</sup>Lu-3PRGD<sub>2</sub>, the <sup>177</sup>Lu-Palm-3PRGD<sub>2</sub> circulation time in blood was more than 6 times longer (slow half-life: 73.42 min versus 11.81 min), and the tumor uptake increased more than fivefold (21.34 ± 4.65 %IA/g and 4.11 ± 0.70 %IA/g at 12 h post-injection). Thus, the significant increase in tumor uptake and tumor retention resulted in enhanced efficacy of targeted radiotherapy, and tumor growth was completely inhibited by a single and relatively low dose of 18.5 MBq/0.5 mCi. Thus, <sup>177</sup>Lu-Palm-3PRGD<sub>2</sub> shows great potential for clinical application.

**Keywords:** <sup>177</sup>Lu; RGD (Arg-Gly-Asp); albumin binder; palmitic acid; peptide receptor radionuclide therapy (PRRT); tumor



**Citation:** Yang, G.; Gao, H.; Luo, C.; Zhao, X.; Luo, Q.; Shi, J.; Wang, F. Palmitic Acid-Conjugated Radiopharmaceutical for Integrin  $\alpha_v\beta_3$ -Targeted Radionuclide Therapy. *Pharmaceutics* **2022**, *14*, 1327. <https://doi.org/10.3390/pharmaceutics14071327>

Academic Editors: Roger Schibli, Iman Kaviani and Makhdoom Sarwar

Received: 13 April 2022

Accepted: 21 June 2022

Published: 23 June 2022

**Publisher's Note:** MDPI stays neutral with regard to jurisdictional claims in published maps and institutional affiliations.



**Copyright:** © 2022 by the authors. Licensee MDPI, Basel, Switzerland. This article is an open access article distributed under the terms and conditions of the Creative Commons Attribution (CC BY) license (<https://creativecommons.org/licenses/by/4.0/>).

## 1. Introduction

Peptide receptor radionuclide therapy (PRRT) is a promising treatment for patients with unresectable or metastatic tumors and has been widely used in clinical practice [1]. Currently, somatostatin analog (SSA)-mediated radionuclide targeting therapy is the most commonly used PRRT in clinical practice and has been approved for clinical application in some countries. Although some progress has made in PRRT applied in clinical practice, most radionuclide-labeled peptides for targeted radiotherapy still face insufficient tumor uptake, and the retention of labeled peptides in tumors is not sufficient, thus limiting their therapeutic effect.

Albumin makes up approximately 55–60% of serum proteins, and its biological half-life is reportedly 19 days, which makes it possible to leverage the long circulation half-life of albumin to produce long-acting therapeutics [2–4]. Radiopharmaceuticals conjugated with albumin binders, such as 4-(p-iodophenyl)butyric acid and truncated Evans Blue (EB), have been used in radiotherapy targeting folate receptor [5–7], somatostatin receptor (SSTR) [8,9], integrin  $\alpha_v\beta_3/\alpha_v\beta_5$  [10] and prostate-specific membrane antigen (PSMA) [11–14] and

have achieved significantly prolonged blood circulation, with enhanced tumor suppression [3,15]. In addition to these well-studied albumin binding groups, fatty acids have also been demonstrated to be typical albumin binding groups and are easy to modify, have affinity of various strengths with albumin and have strong cell membrane penetration ability [16–19]. Recently, Zhang et al., successfully improved the tumor uptake and retention of fibroblast activation protein inhibitor (FAPI) tracers by introducing fatty acids (lauric acid and palmitic acid), as albumin binders [20]. Fatty acid-conjugated peptide drugs, such as Levemir, Tresiba and liraglutide, have been approved by the FDA for clinical use, and they have been found to achieve long-term effects through the binding of fatty acids to albumin, prolonging the blood circulation of insulin and glucagon-like peptide-1 analogs [21]. Therefore, the use of fatty acids as albumin binders is a promising strategy for development of peptide-based radiopharmaceuticals as long-term tumor-targeted radiotherapy agents for clinical application.

Integrin  $\alpha_v\beta_3/\alpha_v\beta_5$  is highly upregulated during tumor angiogenesis and in some tumor cells but not in quiescent vessels and normal organ systems, making it an ideal tumor target for receptor-mediated broad-spectrum tumor-targeting imaging and therapy [22,23]. Many integrin  $\alpha_v\beta_3/\alpha_v\beta_5$ -targeted RGD peptide radiopharmaceuticals have been developed and are widely used in clinical practice [24–27]. Our  $^{99m}\text{Tc}$ -labeled 3PRGD<sub>2</sub> has been clinically used as a diagnostic tracer for early detection of various tumors, and its clinical phase III study has been completed [28–30]. In a previous study, we prepared  $^{177}\text{Lu}$ -labeled 3PRGD<sub>2</sub> and carried out PRRT studies in animal model. Although as a targeted radiotherapy agent,  $^{177}\text{Lu}$ -labeled 3PRGD<sub>2</sub> showed considerable therapeutic efficacy in mouse tumor model, it must be administered twice at a dose of 111 MBq or in combination with Endostar chemotherapy [31]. Its short plasma half-life as well as insufficient tumor uptake and retention time limit its further clinical application. Therefore, we wondered whether introduction of fatty acids could improve the therapeutic effect of  $^{177}\text{Lu}$ -3PRGD<sub>2</sub>.

Since palmitic acid is the most common fatty acid used for drug modification to obtain long circulation drugs, we introduced palmitic acid (termed palm) into the [ $^{177}\text{Lu}$ ]Lu-DOTA-3PRGD<sub>2</sub> structure to obtain [ $^{177}\text{Lu}$ ]Lu-DOTA-Palm-3PRGD<sub>2</sub> and evaluated its potential for targeted radiotherapy in a mouse tumor model. We expected that the introduction of palmitic acid would significantly prolong the blood half-life of  $^{177}\text{Lu}$ -3PRGD<sub>2</sub> and significantly increase the effective dose of  $^{177}\text{Lu}$ -3PRGD<sub>2</sub> and its duration of action in tumors, thus achieving complete tumor elimination at a low dose. Due to the broad-spectrum expression of the integrin receptor, this long-acting RGD radiotherapy agent has broad application prospects in targeted radiotherapy for a variety of tumors.

## 2. Materials and Methods

### 2.1. Materials

Chemicals and solvents were purchased from Sigma-Aldrich (St. Louis, MO, USA). Fmoc-Lys(palmitoyl-Glu-OtBu)-OH was purchased from GlpBio (Montclair, CA, USA). The bifunctional chelator 1,4,7,10-tetraazacyclododecane-1,4,7,10-tetraacetic acid mono-N-hydroxysuccinimide ester (DOTA-NHS ester) was purchased from Macrocyclics Inc. (Dallas, TX, USA). PEG<sub>4</sub>-E[PEG<sub>4</sub>-c(RGDfK)]<sub>2</sub> (termed 3PRGD<sub>2</sub>) was obtained from CS BIO (Menlo Park, CA, USA).  $^{177}\text{LuCl}_3$  solution was purchased from ITG (Schwaig, Germany).

### 2.2. Chemical Synthesis of Conjugates

The synthetic routes of DOTA-Lys(palmitoyl-Glu-OH)-3PRGD<sub>2</sub> (termed DOTA-Palm-3PRGD<sub>2</sub>), DOTA-3PRGD<sub>2</sub>, and DOTA-Lys(palmitoyl-Glu-OH)-OH (termed DOTA-Palm) are shown in the Supporting Information in Figures S1–S3. The preparation procedures are described below. The products were analyzed and isolated using an Agilent 1260 HPLC system equipped with a semipreparative C4 column (Sepax Bio-C4, 10 mm × 250 mm, 5  $\mu\text{m}$ ) and a UV/Vis detector ( $\lambda = 210 \text{ nm}$  or  $254 \text{ nm}$ ). The mobile phase was composed of phase A (0.05% TFA in water) and phase B (0.05% TFA in acetonitrile). The flow rate was 3.2 mL/min, and the phase B gradients are described in the preparation procedures.

### 2.2.1. Synthesis of DOTA-Palm-3PRGD<sub>2</sub>

Synthesis of Fmoc-Lys(palmitoyl-Glu-OtBu)-NHS. Fmoc-Lys(palmitoyl-Glu-OtBu)-OH (20.0 mg, 1.0 eq), 1-ethyl-3-(3-(dimethylamino)propyl)-carbodiimide hydrochloride (EDC·HCl) (7.3 mg, 1.5 eq), and N-hydroxysuccinimide (5.8 mg, 2.0 eq) were dissolved in 1.0 mL dimethylformamide (DMF). The reaction mixture was stirred at room temperature overnight. The product was separated via HPLC (the phase B gradient started from 45% at 0 min to 80% at 25 min and was increased to 45% at 30 min, Method 1). The fraction at 25.8 min was collected and lyophilized to afford Fmoc-Lys(palmitoyl-Glu-OtBu)-NHS. The yield was 19.3 mg (~86%). ESI-MS:  $m/z = 912.72$  for  $[M + Na]^+$  ( $M = 889.14$  calcd for  $[C_{50}H_{72}N_4O_{10}]$ ).

Synthesis of Lys(palmitoyl-Glu-OH)-3PRGD<sub>2</sub>. Fmoc-Lys(palmitoyl-Glu-OtBu)-NHS (5.0 mg, 1.0 eq) and 3PRGD<sub>2</sub> (11.6 mg, 1 eq) were dissolved in 200  $\mu$ L DMF. After the addition of DIEA to adjust the solution pH to 8.0, the mixture was stirred at room temperature overnight. The product was separated via HPLC (Method 1), and the fraction at 17.6 min was collected and lyophilized to afford Fmoc-Lys(palmitoyl-Glu-OtBu)-3PRGD<sub>2</sub>. The product (5 mg) was dissolved in 400  $\mu$ L of TFA, stirred at room temperature for 5 min and then blown dry with nitrogen. The reaction product was dissolved in 100  $\mu$ L DMF. After addition of 25  $\mu$ L piperidine, the mixture was stirred at room temperature for 10 min. The product was separated via HPLC (Method 1). The fraction at 12.7 min was collected and lyophilized to afford Lys(palmitoyl-Glu-OH)-3PRGD<sub>2</sub>. The yield was 2.7 mg (~60%). MALDI-TOF-MS:  $m/z = 2555.71$  for  $[M + H]^+$  ( $M = 2554.45$  calcd for  $[C_{119}H_{199}N_{25}O_{36}]$ ).

Synthesis of DOTA-Palm-3PRGD<sub>2</sub>. Lys(palmitoyl-Glu-OH)-3PRGD<sub>2</sub> (1.3 mg, 1 eq) and DOTA-NHS ester (0.41 mg, 1.6 eq) were dissolved in 200  $\mu$ L DMF. After the addition of DIEA to adjust the solution pH to 8.0, the mixture was stirred at room temperature overnight. The product was separated via HPLC (Method 1), and the fraction at 11.9 min was collected and lyophilized to afford DOTA-Palm-3PRGD<sub>2</sub>. The yield was 0.6 mg (~40%). MALDI-TOF-MS:  $m/z = 2941.25$  for  $[M + H]^+$  ( $M = 2940.63$  calcd for  $[C_{135}H_{225}N_{29}O_{43}]$ ).

### 2.2.2. Synthesis of DOTA-3PRGD<sub>2</sub>

3PRGD<sub>2</sub> (2.0 mg, 1 eq) and DOTA-NHS ester (0.73 mg, 1.5 eq) were dissolved in 200  $\mu$ L DMF. After the addition of DIEA to adjust the solution pH to 8.0, the mixture was stirred at room temperature overnight. The product was separated via HPLC. The mobile phase was isocratic with 90% phase A and 10% phase B at 0–5 min, followed by a mobile phase gradient from 10% phase B at 5 min to 60% at 25 min and to 10% at 30 min (Method 2). The fraction at 18.0 min was collected and lyophilized to afford DOTA-3PRGD<sub>2</sub>. The yield was 1.2 mg (~50%). MALDI-TOF-MS:  $m/z = 2446.02$  for  $[M + H]^+$  ( $M = 2445.26$  calcd for  $[C_{108}H_{176}N_{26}O_{38}]$ ).

### 2.2.3. Synthesis of DOTA-Palm

Fmoc-Lys(palmitoyl-Glu-OtBu)-OH (5 mg) was dissolved in 200  $\mu$ L TFA. The mixture was stirred at room temperature for 5 min and then blown dry with nitrogen. The reaction product was dissolved in 100  $\mu$ L DMF. After addition of 25  $\mu$ L piperidine, the mixture was stirred at room temperature for 10 min. The product was separated by HPLC. The mobile phase was isocratic with 70% phase A and 30% phase B at 0–5 min, followed by a mobile phase gradient from 30% phase B at 5 min to 80% at 25 min and to 30% at 30 min (Method 3). The fraction at 19.5 min was collected and lyophilized to afford Lys(palmitoyl-Glu-OH)-OH. The product (1.0 mg, 1 eq) and DOTA-NHS ester (1.46 mg, 1.5 eq) were dissolved in 200  $\mu$ L DMF. After addition of DIEA to adjust the solution pH to 8.0, the mixture was stirred at room temperature overnight. The product was separated via HPLC (Method 3). The fraction at 18.9 min was collected and lyophilized to afford DOTA-Palm. The yield was 0.8 mg (~45.7%). MALDI-TOF-MS:  $m/z = 900.41$  for  $[M]^+$  ( $M = 899.56$  calcd for  $[C_{43}H_{77}N_7O_{13}]$ ).

### 2.3. Radiochemistry and In Vivo Stability

DOTA-Palm-3PRGD<sub>2</sub> (40 µg/5 µL DMSO, 13.6 nmol), DOTA-3PRGD<sub>2</sub> (40 µg/5 µL H<sub>2</sub>O, 16.3 nmol), or DOTA-Palm (15 µg/5 µL DMSO, 16.7 nmol) was added to a mixture of 200 µL NH<sub>4</sub>OAc buffer (0.1 M, pH = 4.8) and 20 µL [<sup>177</sup>Lu]LuCl<sub>3</sub> solution (~185 MBq/5 mCi). Next, the vials were heated in an air bath at 100 °C for 25 min. After cooling to room temperature, the radiopharmaceuticals were analyzed with an Agilent 1260 HPLC system equipped with a radioactive detector and a C18 column (YMC-Pack ODS-A, 250 × 4.6 mm, I.D. 5 µm, 12 nm). The flow rate was 1 mL/min. The gradient mobile phase started from 30% phase B at 0 min and progressed to 70% phase B at 25 min and 30% phase B at 30 min. To evaluate in vivo stability, [<sup>177</sup>Lu]-Palm-3PRGD<sub>2</sub> (37 MBq, 2.7 nmol) was injected via the tail vein, and urine samples were collected and analyzed using radio-HPLC at 1 and 6 h post-injection (p.i.).

### 2.4. n-Octanol/PBS Distribution Coefficient

The n-octanol/PBS distribution coefficients of [<sup>177</sup>Lu]-Palm-3PRGD<sub>2</sub>, [<sup>177</sup>Lu]-3PRGD<sub>2</sub>, and [<sup>177</sup>Lu]Lu-DOTA-Palm ([<sup>177</sup>Lu]-Palm) in an n-octanol/PBS system were determined as previously reported [32]. Briefly, the radiopharmaceuticals were prepared and purified with Sep-Pak-C18 cartridges and then dissolved in a mixed solution of 5 mL n-octanol and 5 mL PBS. After vortexing for 1 h, the mixture was centrifuged at 10,000 rpm for 10 min. Samples (100 µL, n = 4) from the n-octanol and PBS components were collected and counted using a γ-counter. The cpm values were calculated as the logarithm of the n-octanol/PBS ratio.

### 2.5. Blood Clearance Study

Female KM mice were randomly divided into three groups (n = 5). Each group was injected intravenously with 0.74 MBq [<sup>177</sup>Lu]-Palm-3PRGD<sub>2</sub>, [<sup>177</sup>Lu]-3PRGD<sub>2</sub>, or [<sup>177</sup>Lu]-Palm. Blood samples obtained from the canthus vein were collected at different time points post injection (p.i.), weighed, and evaluated using a γ-counter. The results are presented as the percentage injected activity per gram (%IA/g). Nonlinear regression (curve fit) followed by two phase decay was performed using GraphPad Prism version 9.0.0 for Windows, GraphPad Software, San Diego, CA, USA, [www.graphpad.com](http://www.graphpad.com) (accessed on 22 May 2022). And then the half-lives values were calculated and determined.

### 2.6. Cell Culture and Animal Model

The human glioma U87MG (ATCC<sup>®</sup> HTB-14<sup>™</sup>) cell lines were purchased from the American Type Culture Collection (ATCC, Manassas, VA, USA). The murine colon adenocarcinoma MC38 cell lines were kindly provided by the lab of Prof. Yangxin Fu at the Institute of Biophysics, Chinese Academy of Sciences (Beijing, China). U87MG and MC38 cells were cultured in Dulbecco's modified Eagle's medium (DMEM) with 10% fetal bovine serum at 37 °C in a humidified atmosphere containing 5% CO<sub>2</sub>. Female C57BL/6 mice (6 weeks of age) were purchased from Beijing Vital River Laboratory Animal Technology Co., Ltd. An MC38 tumor model was established via subcutaneous injection of MC38 cells (1.0 × 10<sup>6</sup>) into the right front flank. When the tumor volume reached the size of 60~100 mm<sup>3</sup>, the mice were used for a targeted radionuclide therapy study. When the tumor volume reached 150~200 mm<sup>3</sup>, the mice were used for a biodistribution study and SPECT/CT imaging. All animal experiments were performed in accordance with the guidelines of the Institutional Animal Care and Use Committee (IACUC) of Peking University.

### 2.7. Cell Uptake Assay

Integrin α<sub>v</sub>β<sub>3</sub>/α<sub>v</sub>β<sub>5</sub>-positive U87MG glioma cells were seeded into a 6-well plate. Then, the cells were incubated with [<sup>177</sup>Lu]-Palm-3PRGD<sub>2</sub> (0.74 MBq, 0.054 nmol) or [<sup>177</sup>Lu]-3PRGD<sub>2</sub> (0.74 MBq, 0.065 nmol) in 1 mL fresh medium (containing the binding ions 20 mM Tris, 150 mM NaCl, 2 mM CaCl<sub>2</sub>, 1 mM MgCl<sub>2</sub>, and 1 mM MnCl<sub>2</sub>; pH = 7.4; without FBS) at 37 °C for 1, 4, or 24 h. Then, the medium was removed, and the cells were washed three

times with ice-cold PBS. Finally, the cells were lysed with 0.5 mL 0.5 M NaOH twice, and the NaOH solution (0.5 mL  $\times$  2) was collected for  $\gamma$ -count determination. The results are presented as a percentage of the added dose per million cells (%AD/ $10^6$  cells).

### 2.8. Competition Binding Assays of $^{177}\text{Lu}$ -Palm-3PRGD<sub>2</sub> and $^{177}\text{Lu}$ -3PRGD<sub>2</sub>

The binding affinity of DOTA-Palm-3PRGD<sub>2</sub> and DOTA-3PRGD<sub>2</sub> to integrin  $\alpha_v\beta_3/\alpha_v\beta_5$  was determined using U87MG glioma cells. Filter multiscreen DV plates were seeded with  $10^5$  U87MG cells in binding buffer (20 mM Tris, 150 mM NaCl, 2 mM CaCl<sub>2</sub>, 1 mM MgCl<sub>2</sub>, 1 mM MnCl<sub>2</sub>, pH = 7.4) and incubated at 4 °C with  $^{177}\text{Lu}$ -Palm-3PRGD<sub>2</sub> or  $^{177}\text{Lu}$ -3PRGD<sub>2</sub> in the presence of increasing concentrations of unlabeled 3PRGD<sub>2</sub>. Meanwhile, U87MG cells were also incubated with  $^{177}\text{Lu}$ -Palm-3PRGD<sub>2</sub> and unlabeled 3PRGD<sub>2</sub> in the presence of human serum albumin (HSA) at 4 °C. After removal of the unbound radiolabeled tracers and several washes with ice-cold PBS, the hydrophilic PVDF filters were collected. Radioactivity was determined using a  $\gamma$ -counter. Nonlinear regression (curve fit) followed by one-site specific binding was performed using GraphPad Prism version 9.0.0. Then the IC<sub>50</sub> values were calculated and determined.

### 2.9. Biodistribution Study

Mice bearing MC38 xenografts were randomly divided into 10 groups ( $n = 4$ ). The mice in five groups were administered 0.74 MBq/20  $\mu\text{Ci}$  of  $^{177}\text{Lu}$ -Palm-3PRGD<sub>2</sub> and sacrificed at 1, 4, 12, 24, and 72 h p.i. The mice on one group was injected with 0.74 MBq/20  $\mu\text{Ci}$  of  $^{177}\text{Lu}$ -Palm-3PRGD<sub>2</sub> and 500  $\mu\text{g}$  (242 nmol) 3PRGD<sub>2</sub> as a blocking agent and sacrificed at 1 h p.i. The mice in the four remaining groups were administered 0.74 MBq/20  $\mu\text{Ci}$  of  $^{177}\text{Lu}$ -Palm or  $^{177}\text{Lu}$ -3PRGD<sub>2</sub> and sacrificed at 4 and 12 h p.i. Tumors and major organs were harvested, weighed and measured for radioactivity using a  $\gamma$ -counter. The organ uptake was calculated as the percentage injected activity per gram (%IA/g). The effective absorbed dose in humans estimated from mouse biodistribution data by using a dedicated software (OLINDA 1.0).

### 2.10. Small-Animal SPECT/CT Imaging

SPECT/CT imaging was performed using a small animal SPECT/CT imaging system (Mediso Inc., Budapest, Hungary). Each mouse bearing MC38 tumors was injected with a radiotracer at a radioactivity of 37 MBq/1 mCi. The mice were imaged at 1, 4, 12, 24, and 72 h after injection of  $^{177}\text{Lu}$ -Palm-3PRGD<sub>2</sub> (37 MBq, 2.7 nmol), and the mice in the blocking study were imaged at 1 h p.i. The mice were imaged at 1 and 4 h after injection of  $^{177}\text{Lu}$ -3PRGD<sub>2</sub> (37 MBq, 3.3 nmol) or  $^{177}\text{Lu}$ -Palm (37 MBq, 3.3 nmol). Pinhole SPECT images (peak, 56.1, 112.9, and 208.4 keV; 20% width; frame time, 25 s) were acquired, and CT images were subsequently acquired (50 kV; 0.67 mA; rotation, 210°; exposure time, 300 ms). The raw data were reconstructed in a whole-body region. The SPECT and CT images were then fused using Nucline v 2.01 (Mediso Inc., Budapest, Hungary). The maximum intensity projection (MIP) was determined for whole-body imaging from the posterior view.

### 2.11. Targeted Radionuclide Therapy

To assess and compare the therapeutic potential of  $^{177}\text{Lu}$ -Palm-3PRGD<sub>2</sub>,  $^{177}\text{Lu}$ -3PRGD<sub>2</sub> and  $^{177}\text{Lu}$ -Palm, MC38 tumor models were used. MC38 tumor-bearing mice with a tumor size of 60–100 mm<sup>3</sup> were randomly divided into four groups (6–8 mice/group). The mice were injected via the tail vein with a single dose injection of saline (as a control), 18.5 MBq/0.5 mCi of  $^{177}\text{Lu}$ -Palm-3PRGD<sub>2</sub> (1.35 nmol),  $^{177}\text{Lu}$ -3PRGD<sub>2</sub> (1.6 nmol) or  $^{177}\text{Lu}$ -Palm (1.7 nmol), respectively. Tumor dimensions and body weight were measured every two or three days. The tumor volume was calculated as  $1/2(\text{length} \times \text{width} \times \text{width})$ . Mice were euthanized when the body weight lost >20% of the original weight. Major organs (heart, lung, liver, spleen and kidney) were harvested at the end of the treatment

study and evaluated for potential toxicity using standard hematoxylin and eosin (H & E) staining analysis.

### 2.12. Statistical Analysis

Numerical results are reported as the mean  $\pm$  standard deviation. Means were compared using Student's *t*-test or multiple unpaired *t*-test. *p*-values  $< 0.05$  were considered statistically significant. \* indicates  $p < 0.05$ , \*\* indicates  $p < 0.01$ , \*\*\* indicates  $p < 0.001$ , and \*\*\*\* indicates  $p < 0.0001$ .

## 3. Results

### 3.1. Chemical Synthesis and Radiolabeling

Detailed synthetic results for DOTA-Palm-3PRGD<sub>2</sub>, DOTA-3PRGD<sub>2</sub>, and DOTA-Palm are shown in the Supplemental Information (Figures S1–S3). DOTA-Palm-3PRGD<sub>2</sub>, DOTA-3PRGD<sub>2</sub> and DOTA-Palm were obtained with more than 95% purity (Figures S4 and S5) and confirmed by MALDI-TOF-MS (Figures S6–S8). All <sup>177</sup>Lu-labeled radiopharmaceuticals were prepared by reacting <sup>177</sup>LuCl<sub>3</sub> with the respective DOTA conjugate (DOTA-Palm-3PRGD<sub>2</sub>, DOTA-3PRGD<sub>2</sub>, and DOTA-Palm) in NH<sub>4</sub>OAc buffer (0.1 M, pH = 4.8) at 100 °C for 25 min. Schematic structures of radiopharmaceuticals are shown in Figure 1. The radiochemical purities were  $>95\%$ , with a molar activity of 13.6 MBq/0.37 mCi per nmol, 11.1 MBq/nmol and 11.3 MBq/nmol for <sup>177</sup>Lu-Palm-3PRGD<sub>2</sub>, <sup>177</sup>Lu-Palm and <sup>177</sup>Lu-3PRGD<sub>2</sub>, respectively (Figure S9). <sup>177</sup>Lu-Palm-3PRGD<sub>2</sub> showed satisfactory *in vivo* stability (Figure S9B).

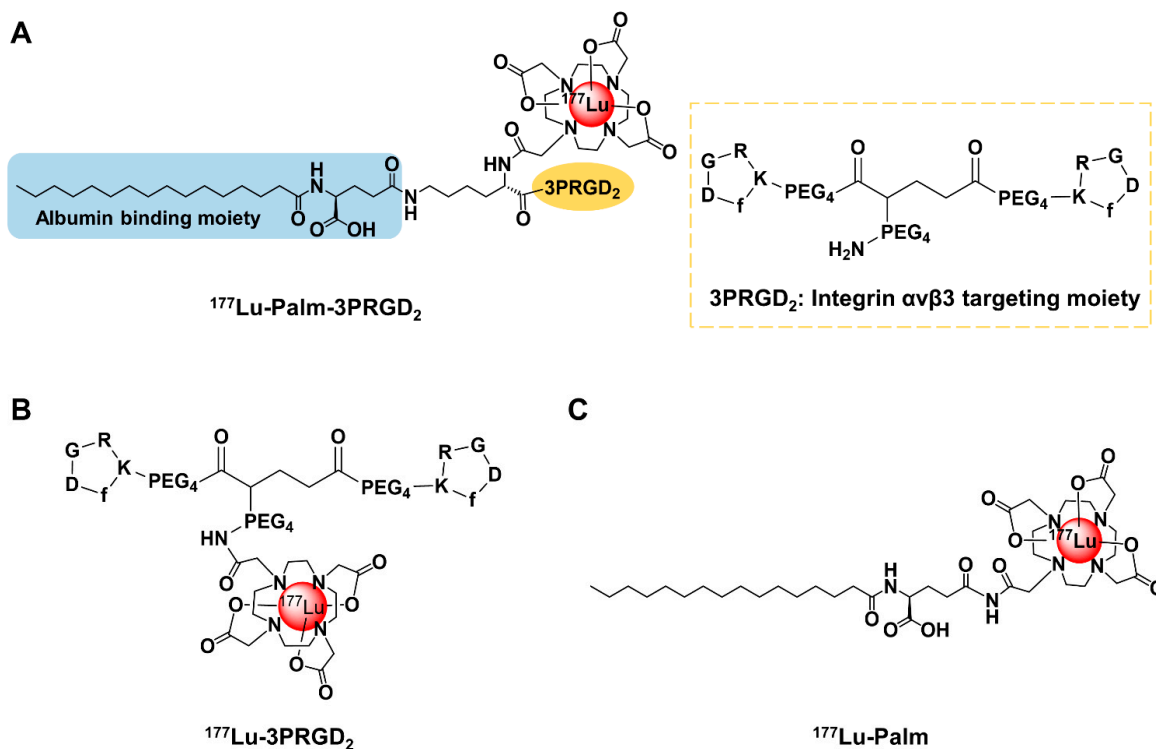


**Figure 1.** Schematic structures of (A) <sup>177</sup>Lu-Palm-3PRGD<sub>2</sub>, (B) <sup>177</sup>Lu-3PRGD<sub>2</sub>, and (C) <sup>177</sup>Lu-Palm. Palmitic acid, as an albumin-binding moiety, is marked with a blue shadow. Integrin  $\alpha_v\beta_3/\alpha_v\beta_5$ -targeting 3PRGD<sub>2</sub> is marked with a yellow shadow.

### 3.2. *n*-Octanol/PBS Distribution Coefficient ( $\log P_{O/W}$ )

The  $\log P_{O/W}$  values of <sup>177</sup>Lu-Palm-3PRGD<sub>2</sub>, <sup>177</sup>Lu-3PRGD<sub>2</sub> and <sup>177</sup>Lu-Palm were determined to be  $-1.25 \pm 0.07$ ,  $-4.05 \pm 0.14$  and  $5.93 \pm 0.01$ , respectively (Table 1). This result is consistent with the trend of the radiopharmaceutical retention time analyzed via radio-HPLC (22.07, 5.05 and 25.13 min, respectively). These results indicate that the introduction of palmitic acid increased the hydrophobicity of the conjugated tracer, but

due to the high hydrophilicity of 3PRGD<sub>2</sub>, the resulting radiopharmaceutical still had an appropriate n-octanol/PBS distribution coefficient.

**Table 1.** LogP<sub>O/W</sub> values and HPLC retention time of <sup>177</sup>Lu-Palm-3PRGD<sub>2</sub>, <sup>177</sup>Lu-3PRGD<sub>2</sub> and <sup>177</sup>Lu-Palm.

	<sup>177</sup> Lu-Palm-3PRGD <sub>2</sub>	<sup>177</sup> Lu-3PRGD <sub>2</sub>	<sup>177</sup> Lu-Palm
Log P <sub>O/W</sub>	-1.25 ± 0.07	-4.05 ± 0.14	5.93 ± 0.01
HPLC retention time/min	22.07	5.05	25.13

### 3.3. Blood Clearance Study

Blood clearance studies were performed in normal KM mice. The blood clearance curves and half-lives of <sup>177</sup>Lu-Palm-3PRGD<sub>2</sub>, <sup>177</sup>Lu-3PRGD<sub>2</sub> and <sup>177</sup>Lu-Palm are shown in Figure 2A and Table 2. <sup>177</sup>Lu-3PRGD<sub>2</sub> showed a particularly fast blood clearance ( $T_{1/2\alpha} = 1.94$  min;  $T_{1/2\beta} = 11.81$  min), <sup>177</sup>Lu-Palm showed prolonged blood retention ( $T_{1/2\alpha} = 3.33$  min;  $T_{1/2\beta} = 29.82$  min), and <sup>177</sup>Lu-Palm-3PRGD<sub>2</sub> had the longest blood half-life ( $T_{1/2\alpha} = 4.49$  min;  $T_{1/2\beta} = 73.42$  min). The result of area under the curve (AUC) analysis further suggested that <sup>177</sup>Lu-Palm-3PRGD<sub>2</sub> (AUC = 4002.00) had significantly improved blood retention capacity compared with <sup>177</sup>Lu-3PRGD<sub>2</sub> (AUC = 430.30) and <sup>177</sup>Lu-Palm (AUC = 1611.00). Blood clearance studies were also performed in C57BL/6 mice. The blood clearance curves and half-lives of <sup>177</sup>Lu-Palm-3PRGD<sub>2</sub> and <sup>177</sup>Lu-3PRGD<sub>2</sub> are shown in the Supplemental Information (Figure S10). <sup>177</sup>Lu-Palm-3PRGD<sub>2</sub> also demonstrated significantly longer blood half-life ( $T_{1/2\alpha} = 2.08$  min;  $T_{1/2\beta} = 63.71$  min) than that of <sup>177</sup>Lu-3PRGD<sub>2</sub> ( $T_{1/2\alpha} = 1.06$  min;  $T_{1/2\beta} = 14.54$  min).

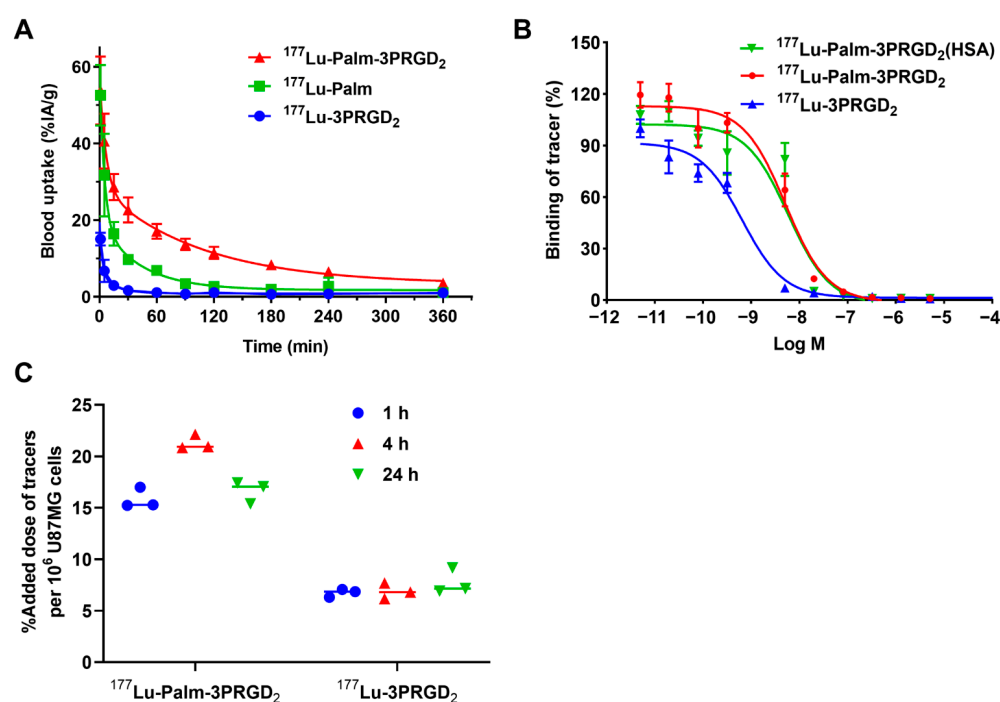


**Figure 2.** In vitro and in vivo characteristics of radiopharmaceuticals. (A) Blood clearance curves of <sup>177</sup>Lu-Palm-3PRGD<sub>2</sub>, <sup>177</sup>Lu-3PRGD<sub>2</sub>, and <sup>177</sup>Lu-Palm performed in KM mice. (B) Competition binding assays of <sup>177</sup>Lu-Palm-3PRGD<sub>2</sub> (in the presence or absence of HSA) and <sup>177</sup>Lu-3PRGD<sub>2</sub> at different assays concentrations of unlabeled 3PRGD<sub>2</sub> peptide. (C) Cell uptake of <sup>177</sup>Lu-Palm-3PRGD<sub>2</sub> and <sup>177</sup>Lu-3PRGD<sub>2</sub> at 1, 4 or 24 h after incubation with integrin  $\alpha_v\beta_3/\alpha_v\beta_5$ -positive U87MG glioma cells.

**Table 2.** Blood Half-life values and AUC values of  $^{177}\text{Lu}$ -Palm-3PRGD<sub>2</sub>,  $^{177}\text{Lu}$ -3PRGD<sub>2</sub> and  $^{177}\text{Lu}$ -Palm.

	$^{177}\text{Lu}$ -Palm-3PRGD <sub>2</sub>	$^{177}\text{Lu}$ -3PRGD <sub>2</sub>	$^{177}\text{Lu}$ -Palm
Half-Life ( $T_{1/2\alpha}$ ) min	4.49	1.94	3.33
Half-Life ( $T_{1/2\beta}$ ) min	73.42	11.81	29.82
AUC (%IA/g·min)	4002.00	430.30	1611.00

### 3.4. Competition Assays

To determine whether palmitic acid conjugation compromised the binding affinity of 3PRGD<sub>2</sub> for integrin  $\alpha_v\beta_3/\alpha_v\beta_5$ , competition binding assays were performed (Figure 2B). The IC<sub>50</sub> values were calculated to be  $0.66 \pm 1.20$  nM for  $^{177}\text{Lu}$ -3PRGD<sub>2</sub> and  $5.13 \pm 1.16$  nM for  $^{177}\text{Lu}$ -Palm-3PRGD<sub>2</sub>. Meanwhile, the IC<sub>50</sub> value for  $^{177}\text{Lu}$ -Palm-3PRGD<sub>2</sub> was  $5.82 \pm 1.29$  nM in the presence of HSA. The binding affinity of 3PRGD<sub>2</sub> for integrin  $\alpha_v\beta_3/\alpha_v\beta_5$  was affected to some extent but was still at the nanomolar level. Notably, the binding affinity of  $^{177}\text{Lu}$ -Palm-3PRGD<sub>2</sub> was not different in the presence or absence of HSA, possibly due to the higher affinity of 3PRGD<sub>2</sub> for integrin  $\alpha_v\beta_3/\alpha_v\beta_5$  than that of palmitic acid for HSA.

### 3.5. Cell Uptake Study

The cellular uptake results for  $^{177}\text{Lu}$ -Palm-3PRGD<sub>2</sub> and  $^{177}\text{Lu}$ -3PRGD<sub>2</sub> are shown in Figure 2C. The uptake of  $^{177}\text{Lu}$ -3PRGD<sub>2</sub> in U87MG tumor cells was  $6.74 \pm 0.39\%$ ,  $6.88 \pm 0.76\%$  and  $7.74 \pm 1.24\%$  after incubation for 1, 4 and 24 h, respectively. The uptake of  $^{177}\text{Lu}$ -Palm-3PRGD<sub>2</sub> was much higher than that of  $^{177}\text{Lu}$ -3PRGD<sub>2</sub>, with values of  $15.84 \pm 1.00\%$ ,  $21.30 \pm 0.72\%$  and  $16.62 \pm 1.08\%$  after incubation for 1, 4 and 24 h, respectively. These results indicate that the introduction of palmitic acid might improve the cellular uptake of  $^{177}\text{Lu}$ -3PRGD<sub>2</sub>.

### 3.6. Small Animal SPECT/CT Imaging

The in vivo properties of  $^{177}\text{Lu}$ -Palm-3PRGD<sub>2</sub>,  $^{177}\text{Lu}$ -3PRGD<sub>2</sub> and  $^{177}\text{Lu}$ -Palm were evaluated using small animal SPECT/CT in MC38 tumor-bearing mice. Representative images of  $^{177}\text{Lu}$ -3PRGD<sub>2</sub> are shown in Figure 3A.  $^{177}\text{Lu}$ -3PRGD<sub>2</sub> was rapidly cleared from circulation and excreted via the renal urinary system. Its tumor uptake was relatively low, and under the same conditions used to visualize tumor uptake of  $^{177}\text{Lu}$ -Palm-3PRGD<sub>2</sub>, the tumors could not be clearly visualized. The mice injected with  $^{177}\text{Lu}$ -Palm-3PRGD<sub>2</sub> were imaged until 72 h p.i., and representative images are presented in Figure 3B. Tumors were clearly visible, and  $^{177}\text{Lu}$ -Palm-3PRGD<sub>2</sub> maintained high accumulation and long retention in tumors from 1 to 72 h p.i. The blood pool uptake of  $^{177}\text{Lu}$ -Palm-3PRGD<sub>2</sub> was obvious from 1 to 4 h p.i., showing long circulation in the blood. A blocking study was performed by co-injecting  $^{177}\text{Lu}$ -Palm-3PRGD<sub>2</sub> with excess unlabeled 3PRGD<sub>2</sub>. SPECT/CT images and quantification of tumor uptake are shown in Figure 3C. The tumor uptake was significantly decreased ( $15.00 \pm 0.13$  %IA/cc vs.  $3.22 \pm 0.13$  %IA/cc,  $p < 0.0001$ ), indicating the active tumor targeting by 3PRGD<sub>2</sub> (Figure 3D). Interestingly,  $^{177}\text{Lu}$ -Palm was barely detectable in the tumors (Figure 3E) and was rapidly distributed from the blood to organs (mainly to the liver) and metabolized, finally accumulating in the gall bladder before being excreted in feces.

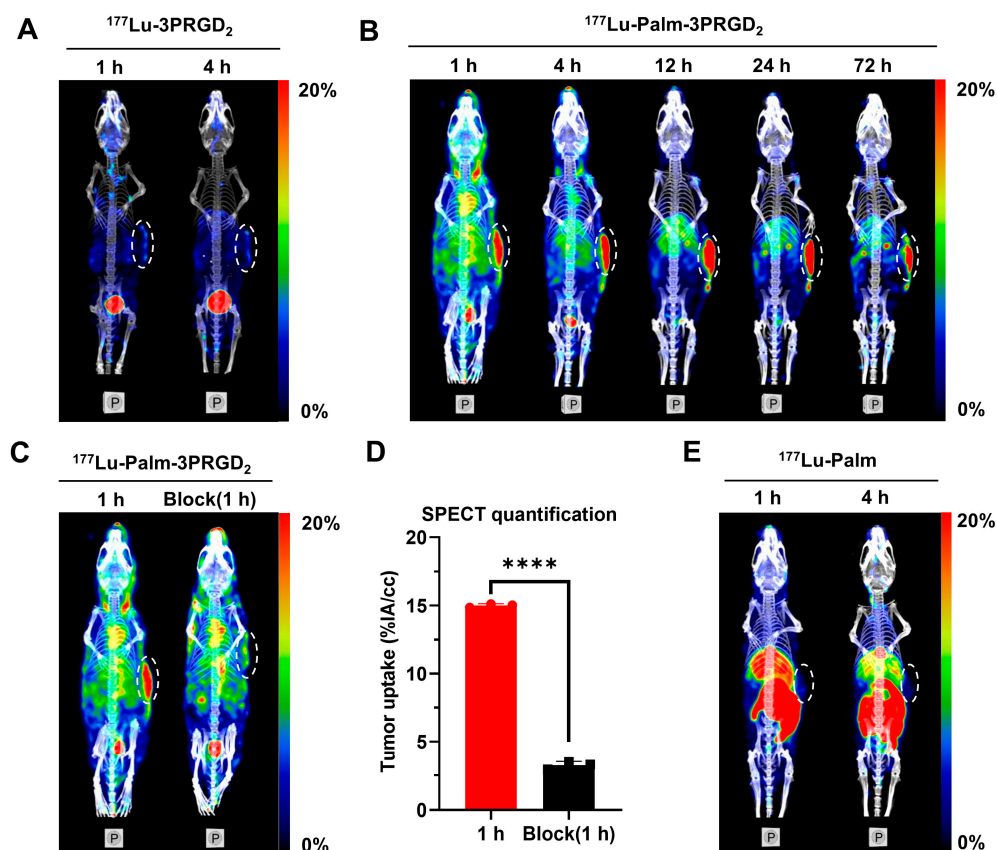


**Figure 3.** Representative nanoScan SPECT/CT images of radiopharmaceuticals in MC38 tumor-bearing mice. The images are posterior views obtained by maximum intensity projection (MIP) and fused with reconstructed CT. (A) Images of  $^{177}\text{Lu}$ -3PRGD<sub>2</sub> at 1 and 4 h p.i. (B) Images of  $^{177}\text{Lu}$ -Palm-3PRGD<sub>2</sub> at 1–72 h p.i. (C) Images of  $^{177}\text{Lu}$ -Palm-3PRGD<sub>2</sub> at 1 h p.i. without or with coinjection of excess unlabeled 3PRGD<sub>2</sub> as a competitor. (D) SPECT quantification of tumor uptake of  $^{177}\text{Lu}$ -Palm-3PRGD<sub>2</sub>. (E) Images of  $^{177}\text{Lu}$ -Palm at 1 and 4 h p.i. All tumors are circled with white dotted lines. The significance indicator \*\*\*\* corresponds to  $p < 0.0001$  determined by Student's *t*-test.

### 3.7. In Vivo Biodistribution Study

The in vivo biodistribution properties of  $^{177}\text{Lu}$ -Palm-3PRGD<sub>2</sub>,  $^{177}\text{Lu}$ -Palm, and  $^{177}\text{Lu}$ -3PRGD<sub>2</sub> were further evaluated in MC38 tumor-bearing mice. The tumor uptake of  $^{177}\text{Lu}$ -Palm-3PRGD<sub>2</sub> increased from  $14.41 \pm 2.53$  to  $26.27 \pm 6.34\%$  IA/g at 1 h and 4 h p.i. and then decreased gradually over time with the values of  $22.91 \pm 4.20$ ,  $17.22 \pm 3.30$ , and  $5.83 \pm 1.27\%$  IA/g at 12, 24 and 72 h p.i. (Figure 4A and Table S1).  $^{177}\text{Lu}$ -Palm-3PRGD<sub>2</sub> was distributed into the main organs within 4 h, resulting in reduced blood pool uptake ( $9.73 \pm 1.16$  to  $4.11 \pm 1.52\%$  IA/g at 1 h and 4 h,  $p = 0.0071$ ). The liver and kidney demonstrated relatively high uptake, with values of  $22.40 \pm 2.55$  and  $20.11 \pm 0.60\%$  IA/g at 4 h p.i., which reduced to  $6.73 \pm 1.18$  and  $10.58 \pm 1.11\%$  IA/g at 72 p.i. Similarly, intestinal uptake was also high, with values of  $20.65 \pm 1.97$  to  $12.80 \pm 1.06\%$  IA/g at 1 h and 72 h p.i. Co-injection of  $^{177}\text{Lu}$ -Palm-3PRGD<sub>2</sub> with excess 3PRGD<sub>2</sub> significantly reduced tumor uptake ( $14.41 \pm 2.53$  vs.  $7.00 \pm 2.47\%$  IA/g,  $p = 0.011$ ) in the blocking study, indicating receptor-mediated uptake (Figure 4B and Table S1). In addition, the intestinal uptake of  $^{177}\text{Lu}$ -Palm-3PRGD<sub>2</sub> was notably reduced in the blocking study ( $20.65 \pm 1.97$  vs.  $7.53 \pm 2.15\%$  IA/g,  $p < 0.01$ ). Otherwise, the blood uptake was significantly higher in the blocking group ( $27.88 \pm 4.66$  vs.  $9.73 \pm 1.16\%$  IA/g,  $p < 0.01$ ) due to reduced distribution from blood to organs (such as the liver, spleen, intestine, and kidney).

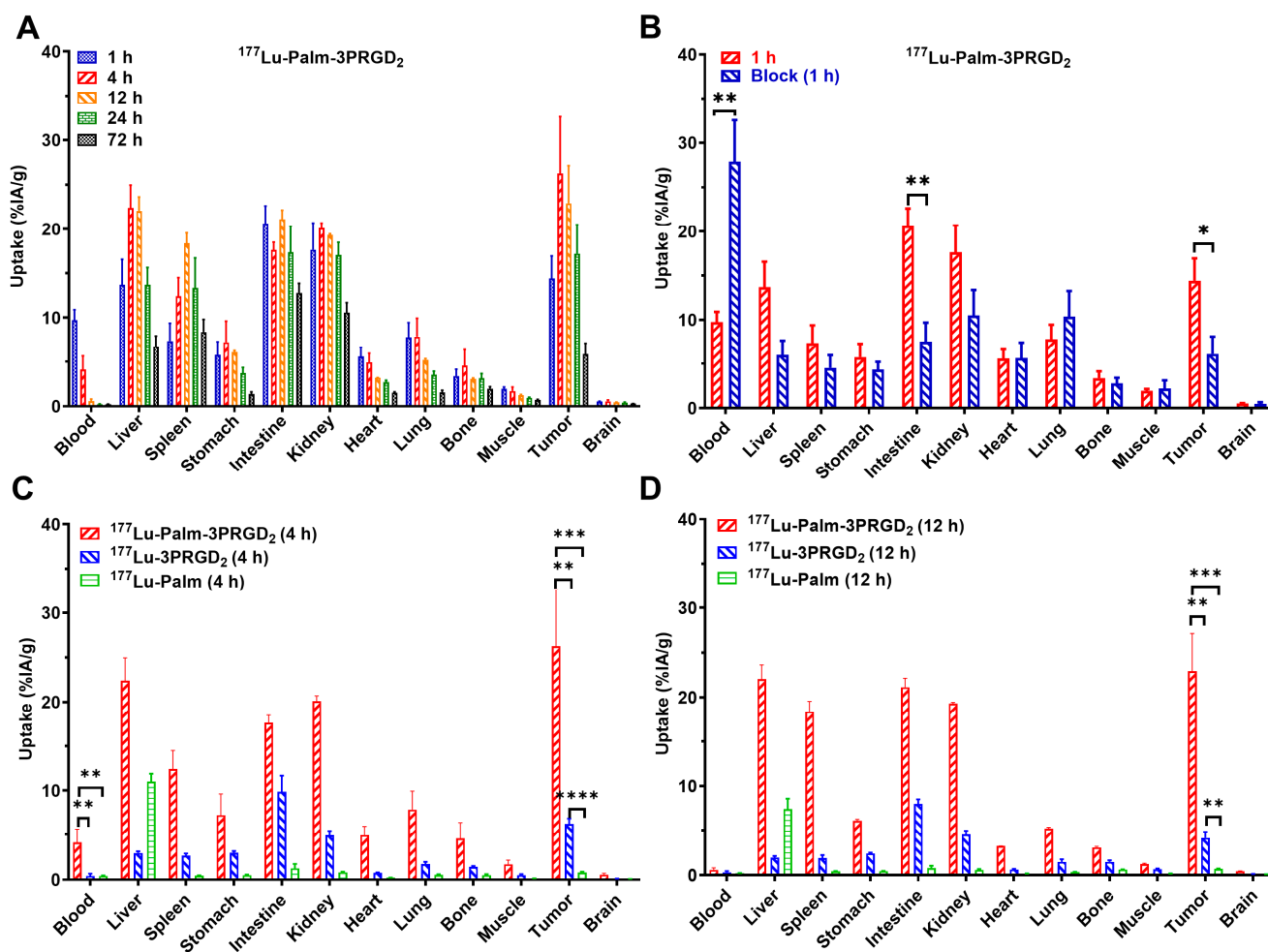


**Figure 4.** Biodistribution of radiopharmaceuticals in MC38 tumor-bearing mice. (A) Biodistribution results for  $^{177}\text{Lu}$ -Palm-3PRGD<sub>2</sub> at 1, 4, 12, 24, and 72 h p.i. (B) Blocking study of  $^{177}\text{Lu}$ -Palm-3PRGD<sub>2</sub> after coinjection of excess unlabeled 3PRGD<sub>2</sub> peptide at 1 h p.i. (C,D) Comparison of the biodistribution results for  $^{177}\text{Lu}$ -Palm-3PRGD<sub>2</sub>,  $^{177}\text{Lu}$ -Palm and  $^{177}\text{Lu}$ -3PRGD<sub>2</sub> at 4 h and 12 p.i., respectively. \* Indicates  $p < 0.05$ , \*\* indicates  $p < 0.01$ , \*\*\* indicates  $p < 0.005$ , and \*\*\*\* indicates  $p < 0.0001$ , determined by multiple unpaired  $t$ -test.

$^{177}\text{Lu}$ -Palm and  $^{177}\text{Lu}$ -3PRGD<sub>2</sub> were evaluated in MC38 tumor-bearing mice at 4 and 12 h p.i. (Figure 4C,D). Compared to  $^{177}\text{Lu}$ -Palm-3PRGD<sub>2</sub>,  $^{177}\text{Lu}$ -3PRGD<sub>2</sub> exhibited relatively lower tumor uptake at 4 and 12 h p.i. (4 h:  $6.22 \pm 0.62$  vs.  $26.27 \pm 6.34\%$  IA/g,  $p = 0.0013$ ; 12 h:  $4.11 \pm 0.70$  vs.  $22.91 \pm 4.20\%$  IA/g,  $p = 0.0003$ ). Due to modification with palmitic acid,  $^{177}\text{Lu}$ -Palm-3PRGD<sub>2</sub> showed increased retention in the blood compared with  $^{177}\text{Lu}$ -3PRGD<sub>2</sub> at 4 h p.i. ( $4.11 \pm 1.52$  vs.  $0.42 \pm 0.26\%$  IA/g,  $p < 0.01$ ), resulting in relatively higher background uptake (Tables S2 and S3). Without the active targeting capability, tumor uptake of  $^{177}\text{Lu}$ -Palm was negligible at 4 and 12 h p.i. ( $0.80 \pm 0.09$  and  $0.68 \pm 0.05\%$  IA/g, respectively).  $^{177}\text{Lu}$ -Palm mainly accumulated in the liver ( $11.00 \pm 0.90$  to  $7.40 \pm 1.15\%$  IA/g at 4 and 12 h p.i.), was metabolized through the gall bladder and was excreted in feces (Figures 3E and 4C,D).

### 3.8. Therapeutic Efficacy of Targeted Radionuclide Therapy

The therapeutic efficacies of  $^{177}\text{Lu}$ -Palm-3PRGD<sub>2</sub>,  $^{177}\text{Lu}$ -3PRGD<sub>2</sub> and  $^{177}\text{Lu}$ -Palm were investigated in immunocompetent mice bearing MC38 tumors. The tumor uptake of  $^{177}\text{Lu}$ -Palm-3PRGD<sub>2</sub> was significantly higher than that of  $^{177}\text{Lu}$ -3PRGD<sub>2</sub> or  $^{177}\text{Lu}$ -Palm at all determined time points (Figure 5A). The uptake of  $^{177}\text{Lu}$ -Palm-3PRGD<sub>2</sub> in tumors and

major organs was calculated as  $AUC_{0h \rightarrow 72h}$  (Figure 5B). The AUC values of  $^{177}\text{Lu}$ -Palm-3PRGD<sub>2</sub> in MC38 tumor and the blood, kidney and liver were  $1031.0 \pm 97.25$ ,  $104.5 \pm 7.98$ ,  $1087.0 \pm 62.73$  and  $915.6 \pm 74.74\%$  IA/g·h, respectively, suggesting high radioactivity accumulation and retention in tumors for targeted radionuclide therapy. The results of targeted radionuclide therapy are illustrated in Figure 5C. Compared to the saline or  $^{177}\text{Lu}$ -Palm group, the  $^{177}\text{Lu}$ -3PRGD<sub>2</sub> and  $^{177}\text{Lu}$ -Palm-3PRGD<sub>2</sub> groups revealed significant tumor inhibition effects. Compared with  $^{177}\text{Lu}$ -3PRGD<sub>2</sub>,  $^{177}\text{Lu}$ -Palm-3PRGD<sub>2</sub> suppressed tumor growth more efficiently due to higher tumor uptake and longer tumor retention. Transient body weight loss was observed in the  $^{177}\text{Lu}$ -Palm-3PRGD<sub>2</sub> group during the initial treatment but then returned to a healthy level at the end of the treatment studies (Figure 5D). No significant body weight loss (>20% loss of the original weight) was observed in any treatment group. H & E staining of the main organs showed negligible toxic effects in all treatment groups (Figure S11).

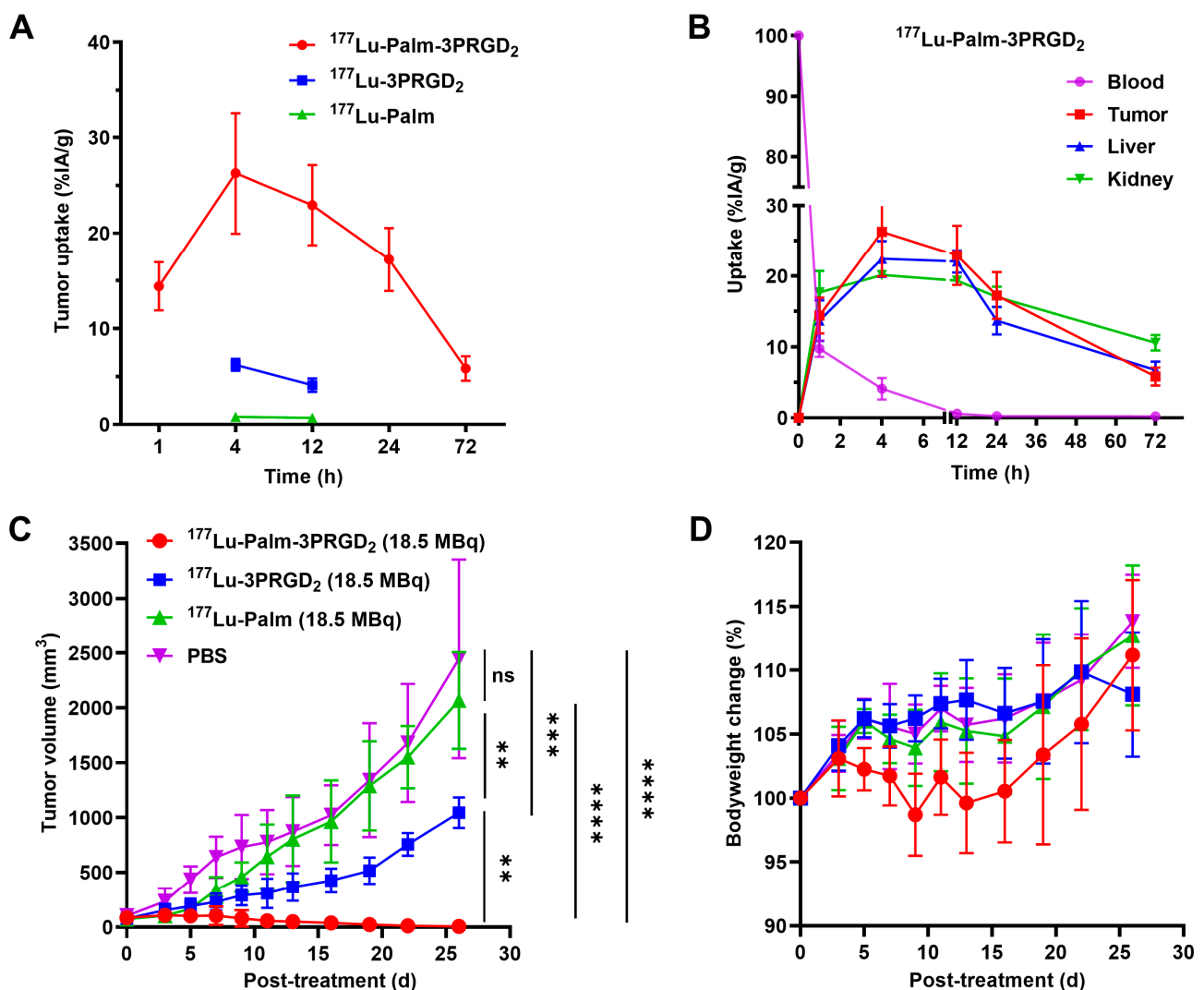


**Figure 5.** (A) Time-activity curves for  $^{177}\text{Lu}$ -Palm-3PRGD<sub>2</sub>,  $^{177}\text{Lu}$ -3PRGD<sub>2</sub>, and  $^{177}\text{Lu}$ -Palm in tumors. The values are based on a biodistribution study. (B) Time-activity curves for  $^{177}\text{Lu}$ -Palm-3PRGD<sub>2</sub> in tumors and major organs. The values are based on a biodistribution study. Tumor growth curves (C) and body weight change curves (D) after targeted radionuclide therapy with PBS (as a control),  $^{177}\text{Lu}$ -Palm-3PRGD<sub>2</sub> (18.5 MBq),  $^{177}\text{Lu}$ -3PRGD<sub>2</sub> (18.5 MBq) or  $^{177}\text{Lu}$ -Palm (18.5 MBq) in C57BL/6 mice bearing established MC38 tumors. ns indicates non-significance, \*\* indicates  $p < 0.01$ , \*\*\* indicates  $p < 0.001$ , and \*\*\*\* indicates  $p < 0.0001$  determined by Student's *t*-test.

#### 4. Discussion

Integrin  $\alpha_v\beta_3/\alpha_v\beta_5$  is specifically overexpressed in tumor neovascularization and a variety of tumor cells, making it an attractive target for the development of broad-spectrum targeted radiopharmaceuticals. Previously,  $^{177}\text{Lu}$ -3PRGD<sub>2</sub>, which targets integrin  $\alpha_v\beta_3/\alpha_v\beta_5$ , was developed for treatment of integrin  $\alpha_v\beta_3/\alpha_v\beta_5$  positive tumors. However, the short blood half-life of  $^{177}\text{Lu}$ -3PRGD<sub>2</sub> resulted in low availability in target organs. This limitation required treatment with higher or more frequent doses ( $111\text{ MBq}/3\text{ mCi} \times 2$ ), both of which may increase the likelihood of adverse side effects [31]. To improve the blood half-life of drugs, drug molecules can be conjugated to albumin-binding molecules to provide an extended half-life in blood [3,10,20]. Fatty acid modified peptide drugs have been widely used in clinical practice as long-acting drugs, which proves that this strategy has great potential for clinical translation [21]. At present, this strategy has not yet been used in the development of RGD radiopharmaceuticals. It is not known whether fatty acid-modified RGD radiopharmaceuticals can be sufficiently effective as long-acting radiopharmaceuticals to achieve enhanced efficacy and attenuated toxicity so that a single low-dose administration can cure tumors, guaranteeing the potential for further clinical translation. Here, we introduced the albumin binder palmitic acid into the  $^{177}\text{Lu}$ -3PRGD<sub>2</sub> peptide structure to obtain the long-acting radiopharmaceutical  $^{177}\text{Lu}$ -Palm-3PRGD<sub>2</sub> and evaluated its therapeutic efficacy in a tumor model.

First, palmitic acid modification inevitably affected the binding affinity or selectivity of 3PRGD<sub>2</sub> to integrin  $\alpha_v\beta_3/\alpha_v\beta_5$ , but the IC<sub>50</sub> value of  $^{177}\text{Lu}$ -palm-3PRGD<sub>2</sub> was still within the nanomolar range. In addition, the cellular uptake of  $^{177}\text{Lu}$ -Palm-3PRGD<sub>2</sub> was much higher than that of  $^{177}\text{Lu}$ -3PRGD<sub>2</sub> in U87MG cells, suggesting that the introduction of palmitic acid might have additional effects on cell uptake. Most likely, hydrophobic interactions between the palmitic acid carbon chain and membrane lipids or lipid rafts potentially distort the outer phospholipid monolayer and accordingly induce palmitic acid internalization and enhance the cellular uptake of tracer [33–35]. The increased cell uptake may also contribute to increased tracer retention in tumors. Western blotting results in Figure S12 showed that U87MG cells and tumor tissues were both positive for integrin  $\alpha_v\beta_3/\alpha_v\beta_5$  expression, while MC38 cells and tumor tissues both had low expression of  $\alpha_v\beta_3$  and no integrin  $\alpha_v\beta_5$  expression, which was consistent with the results of previous studies [31,32,36,37]. We therefore performed in vitro cell competition binding studies using U87MG tumor cells. However, in order to better compare the enhancement of tumor efficacy caused by prolonged drug retention, MC38 cells with relatively low expression of integrin  $\alpha_v\beta_3$  were selected to establish tumor model and evaluate the enhancement of efficacy in vivo. If there is enough curative effect in such models, the curative effect of models with high expression of integrin  $\alpha_v\beta_3/\alpha_v\beta_5$  will be more guaranteed. Moreover, MC38 is a mouse-derived cell line, and the tumor immune microenvironment of MC38 tumor bearing mice is active, which can simulate the therapeutic effect of the patient with immune response in immune-competent mice [38].

Furthermore, the blood half-life of  $^{177}\text{Lu}$ -palm-3PRGD<sub>2</sub> was significantly longer than that of  $^{177}\text{Lu}$ -3PRGD<sub>2</sub> (the AUC was almost 10 times higher), indicating that palmitic acid modification resulted in a significant prolongation of blood circulation time. This may be caused by several factors: first, palmitic acid can reversibly bind to albumin to prolong the blood retention time and reduce the elimination of peptides [21]; second,  $^{177}\text{Lu}$ -palm-3PRGD<sub>2</sub> is amphiphilic and may self-assemble to form tiny nanoparticles (possibly nanospheres or nanofibers) with larger molecular sizes, resulting in longer blood retention times and higher tumor uptake [33,39]. Research on the hydrodynamic characteristics of palmitoylated peptides is limited, and more work is needed to further confirm our hypothesis. In addition to a significantly longer blood circulation time, tumor uptake and tumor retention of  $^{177}\text{Lu}$ -Palm-3PRGD<sub>2</sub> were significantly increased. Its tumor uptake was enhanced not only by the tumor targeting capacity of 3PRGD<sub>2</sub> but also by the albumin carrier characteristics of palmitic acid. The “piggy-back” strategy via reversible albumin binding of palmitic acid prolonged the ligand–receptor binding window and gave the

radiopharmaceuticals more opportunities to bind to target receptors. The tumor uptake and retention of  $^{177}\text{Lu}$ -Palm-3PRGD<sub>2</sub> were significantly increased compared with those of  $^{177}\text{Lu}$ -3PRGD<sub>2</sub> and  $^{177}\text{Lu}$ -Palm, indicating that the effective dose and duration of action of  $^{177}\text{Lu}$ -Palm-3PRGD<sub>2</sub> in tumors were greatly increased, and thus, the therapeutic efficacy of  $^{177}\text{Lu}$ -Palm-3PRGD<sub>2</sub> was significantly enhanced. Total elimination of the tumors was achieved with a single injection of 18.5 MBq/0.5 mCi  $^{177}\text{Lu}$ -Palm-3PRGD<sub>2</sub>. This is significantly better than the efficacy achieved by two injections of 111 MBq/3 mCi  $^{177}\text{Lu}$ -3PRGD<sub>2</sub> in the U87MG tumor model in our previous study [31]. Moreover, the human effective absorbed dose of  $^{177}\text{Lu}$ -Palm-3PRGD<sub>2</sub> ( $4.04 \times 10^{-2}$  mSv/MBq) was estimated from biodistribution data in mice by Olinda software and shown as Table S6 in supplemental material. The effective absorbed dose of  $^{177}\text{Lu}$ -3PRGD<sub>2</sub> previously studied is  $1.35 \times 10^{-2}$  mSv/MBq [31]. Since the injected dose of  $^{177}\text{Lu}$ -Palm-3PRGD<sub>2</sub> is reduced by at least 6 times (18.5 MBq/0.5 mCi vs. 111 MBq/3 mCi  $\times$  2) under a comparable therapeutic effect, its effective absorbed dose in human will be greatly reduced, and its safety will be more guaranteed than  $^{177}\text{Lu}$ -3PRGD<sub>2</sub>.

Notably, increased tumor uptake was accompanied by increased uptake in normal organs, which may lead to tissue damage. This is partially due to increased blood accumulation and circulation time of  $^{177}\text{Lu}$ -Palm-3PRGD<sub>2</sub>, resulting in higher uptake of blood rich organs such as liver and spleen. In addition, palmitic acid itself has high lipophilicity, which will also increase the uptake of metabolic organs such as liver and intestine. The biodistribution results of  $^{177}\text{Lu}$ -Palm confirmed the corresponding high liver and intestinal uptake caused by high lipophilicity. The results of the blocking study indicated that uptake was significantly inhibited in the intestine, liver, and kidney, suggesting that uptake in these tissues may be mediated in part by integrin  $\alpha_v\beta_3/\alpha_v\beta_5$ . In addition, two other regions showed relatively strong radioactivity accumulation at late time points (12, 24, and 72 h p.i.), probably the adrenal glands based on the shape and location of regions of interest, but the exact uptake mechanism remains unclear and requires further verification. This may be related to the introduction of albumin binding molecules, as this phenomenon was not detected in the imaging results of  $^{177}\text{Lu}$ -3PRGD<sub>2</sub>. Although no significant bodyweight loss and no observable tissue damage were found, more confirmation should be performed before further clinical application.

Although encouraging results have been obtained, our study also has some limitations. First, we performed in vitro studies using U87MG cells for binding affinity and specificity evaluation, but we assessed the in vivo characteristics of the probe in C57BL/6 mice bearing MC38 tumor models. Although MC38 tumor models were proved to be suitable for targeted radionuclide therapy [38], in vivo evaluation should also be completed in U87MG tumor model to verify the properties of the probe more convincingly. Second, we studied the blood clearance characteristics of RGD radiopharmaceuticals in KM normal mice, but the biological distribution characteristics of RGD radiopharmaceuticals were determined in C57BL/6 tumor bearing mice. Although these two experiments are independent, the inconsistency of mouse strains will affect the correlation and comparison of data [40]. So we then performed the blood clearance study in C57BL/6 mice and supplemented data in supplementary information (Figure S10). Even though there were some differences between strains,  $^{177}\text{Lu}$ -Palm-3PRGD<sub>2</sub> showed significantly longer blood circulation time than  $^{177}\text{Lu}$ -3PRGD<sub>2</sub> (4–6 times) in both mouse strains. These results confirm that the introduction of palmitic acid has led to a significant increase in the amount and time of blood retention of RGD drugs, but further pharmacokinetic studies are still needed before clinical translation research in the future. Third, we only used the MC38 tumor model in the treatment study, and the efficacy of treatment needs to be verified in more tumor models. In addition, this study only evaluated one therapeutic dose (18.5 MBq/0.5 mCi), and whether similar therapeutic effects can be achieved at  $\sim$ 9 MBq/250  $\mu$ Ci or even lower doses also needs to be further investigated in future work. Furthermore, our present study mainly focused on the development of a novel albumin binder-modified radiopharmaceutical, and the mechanism underlying its tumor growth inhibition remains to be further explored.

## 5. Conclusions

In this study, we designed and synthesized a novel long-acting integrin  $\alpha_v\beta_3/\alpha_v\beta_5$ -targeted radiopharmaceutical for targeted radiotherapy. Conjugation of palmitic acid to 3PRGD<sub>2</sub> markedly extended its blood circulation time and enhanced tumor uptake and retention. The resulting drug conjugate showed remarkable tumor treatment efficacy without observable tissue damage. In conclusion, the introduction of palmitic acid as an albumin binder can be a promising strategy to promote small molecule peptide-based radiopharmaceuticals for targeted radiotherapy of cancer.

**Supplementary Materials:** The following supporting information can be downloaded at: <https://www.mdpi.com/article/10.3390/pharmaceutics14071327/s1>. Method and results of Western Blotting. Figure S1: The synthesis route of DOTA-Palm-3PRGD<sub>2</sub>; Figure S2: The synthesis route of DOTA-3PRGD<sub>2</sub>; Figure S3: The synthesis route of DOTA-Palm; Figure S4: HPLC chromatogram results for the synthesis of DOTA-Palm-3PRGD<sub>2</sub>; Figure S5: HPLC chromatogram results for the synthesis of DOTA-Palm and DOTA-3PRGD<sub>2</sub>; Figure S6: MS analysis of DOTA-Palm-3PRGD<sub>2</sub>; Figure S7: MS analysis of DOTA-3PRGD<sub>2</sub>; Figure S8: MS analysis of DOTA-Palm; Figure S9: (A) Radio-HPLC chromatogram of <sup>177</sup>Lu-Palm-3PRGD<sub>2</sub>, (B) metabolic stability analysis of <sup>177</sup>Lu-Palm-3PRGD<sub>2</sub> in urine collected at 1 and 6 h p.i., and radio-HPLC chromatogram of (C) <sup>177</sup>Lu-Palm and (D) <sup>177</sup>Lu-3PRGD<sub>2</sub>; Figure S10: Blood clearance curves of <sup>177</sup>Lu-Palm-3PRGD<sub>2</sub> and <sup>177</sup>Lu-3PRGD<sub>2</sub> performed in C57BL/6 mice. Figure S11: H&E staining of major organs after the treatment study; Figure S12. Integrin  $\alpha_v\beta_3$  and  $\beta_5$  expression patterns in U87MG and MC38 cell lines and tumor tissues. Table S1: Biodistribution results for <sup>177</sup>Lu-Palm-3PRGD<sub>2</sub> in MC38-tumor bearing mice; Table S2: Comparison of biodistribution results for <sup>177</sup>Lu-Palm-3PRGD<sub>2</sub>, <sup>177</sup>Lu-3PRGD<sub>2</sub>, and <sup>177</sup>Lu-Palm at 4 h p.i. in MC38-tumor bearing mice; Table S3: Comparison of biodistribution results for <sup>177</sup>Lu-Palm-3PRGD<sub>2</sub>, <sup>177</sup>Lu-3PRGD<sub>2</sub>, and <sup>177</sup>Lu-Palm at 12 h p.i. in MC38 tumor-bearing mice; Table S4. Tumor-to-tissue ratios of <sup>177</sup>Lu-Palm-3PRGD<sub>2</sub>; Table S5. Comparison of tumor-to-tissue ratios of radiopharmaceuticals at 4 h and 12 h p.i.; Table S6. Human absorbed effective dose estimates of <sup>177</sup>Lu-Palm-3PRGD<sub>2</sub> obtained from MC38 tumor mice (mSv/MBq, *n* = 4).

**Author Contributions:** Conceptualization, G.Y., J.S. and F.W.; methodology, G.Y., H.G., C.L., X.Z., J.S. and F.W.; formal analysis, G.Y. and J.S.; investigation, G.Y., C.L., X.Z. and J.S.; resources, G.Y., Q.L., J.S. and F.W.; writing—original draft preparation, G.Y.; writing—review and editing, J.S. and F.W.; visualization, G.Y. and J.S.; supervision, H.G., Q.L., J.S. and F.W.; project administration, G.Y. and J.S.; funding acquisition, J.S. and F.W. All authors have read and agreed to the published version of the manuscript.

**Funding:** This research was funded in part by the National Key R&D Program of China (2017YFA0205603 to F.W.), National Natural Science Foundation of China (NSFC) projects (92159201 and 81927802 to F.W.; 81971676 to J.S.), Emergency Key Program of Guangzhou Laboratory, Grant No. EKPG21-16 (F.W.), and Youth Innovation Promotion Association of Chinese Academy of Sciences (YIPACAS) project 2016090 (J.S.).

**Institutional Review Board Statement:** All animal experiments were performed in accordance with the Institutional Animal Care and Use Committee (IACUC) at Peking University. This study was approved on 4 March 2022, and the Ethic Committee approval code is LA2021296.

**Informed Consent Statement:** Not applicable.

**Data Availability Statement:** All data generated or analyzed during this study are included in this published article and its Supplementary Information files.

**Acknowledgments:** The authors appreciate Xiaoda Li, Huiyun Zhao, and Lijun Zhong of the Medical and Healthy Analytical Center of Peking University (Beijing, China) for their help with nanoScan SPECT/CT imaging, cell cultures, and mass spectrometry, respectively.

**Conflicts of Interest:** The authors declare no conflict of interest.

## References

1. Gudkov, S.V.; Shilyagina, N.Y.; Vodeneev, V.A.; Zvyagin, A.V. Targeted Radionuclide Therapy of Human Tumors. *Int. J. Mol. Sci.* **2016**, *17*, 33. [[CrossRef](#)] [[PubMed](#)]
2. Sand, K.M.K.; Bern, M.; Nilsen, J.; Noordzij, H.T.; Sandlie, I.; Andersen, J.T. Unraveling the Interaction between FcRn and Albumin: Opportunities for Design of Albumin-Based Therapeutics. *Front. Immunol.* **2015**, *5*, 682. [[CrossRef](#)] [[PubMed](#)]
3. Lau, J.; Jacobson, O.; Niu, G.; Lin, K.-S.; Benard, F.; Chen, X. Bench to Bedside: Albumin Binders for Improved Cancer Radioligand Therapies. *Bioconjug. Chem.* **2019**, *30*, 487–502. [[CrossRef](#)] [[PubMed](#)]
4. Dumelin, C.E.; Trüssel, S.; Buller, F.; Trachsel, E.; Bootz, F.; Zhang, Y.; Mannocci, L.; Beck, S.C.; Drumea-Mirancea, M.; Seeliger, M.W.; et al. A Portable Albumin Binder from a DNA-Encoded Chemical Library. *Angew. Chem. Int. Ed.* **2008**, *47*, 3196–3201. [[CrossRef](#)] [[PubMed](#)]
5. Mueller, C.; Struthers, H.; Winiger, C.; Zhernosekov, K.; Schibli, R. DOTA Conjugate with an Albumin-Binding Entity Enables the First Folic Acid-Targeted Lu-177-Radionuclide Tumor Therapy in Mice. *J. Nucl. Med.* **2013**, *54*, 124–131. [[CrossRef](#)] [[PubMed](#)]
6. Siwowska, K.; Haller, S.; Bortoli, F.; Benešová, M.; Groehn, V.; Bernhardt, P.; Schibli, R.; Müller, C. Preclinical Comparison of Albumin-Binding Radiofolates: Impact of Linker Entities on the in Vitro and in Vivo Properties. *Mol. Pharm.* **2017**, *14*, 523–532. [[CrossRef](#)]
7. Müller, C.; Guzik, P.; Siwowska, K.; Cohrs, S.; Schmid, R.; Schibli, R. Combining Albumin-Binding Properties and Interaction with Pemetrexed to Improve the Tissue Distribution of Radiofolates. *Molecules* **2018**, *23*, 1465. [[CrossRef](#)]
8. Tian, R.; Jacobson, O.; Niu, G.; Kiesewetter, D.O.; Wang, Z.; Zhu, G.; Ma, Y.; Liu, G.; Chen, X. Evans Blue Attachment Enhances Somatostatin Receptor Subtype-2 Imaging and Radiotherapy. *Theranostics* **2018**, *8*, 735–745. [[CrossRef](#)]
9. Liu, Q.; Zang, J.; Sui, H.; Ren, J.; Guo, H.; Wang, H.; Wang, R.; Jacobson, O.; Zhang, J.; Cheng, Y.; et al. Peptide Receptor Radionuclide Therapy of Late-Stage Neuroendocrine Tumor Patients with Multiple Cycles of <sup>177</sup>Lu-DOTA-EB-TATE. *J. Nucl. Med.* **2021**, *62*, 386–392. [[CrossRef](#)]
10. Chen, H.; Jacobson, O.; Niu, G.; Weiss, I.D.; Kiesewetter, D.O.; Liu, Y.; Ma, Y.; Wu, H.; Chen, X. Novel “Add-On” Molecule Based on Evans Blue Confers Superior Pharmacokinetics and Transforms Drugs to Theranostic Agents. *J. Nucl. Med.* **2017**, *58*, 590–597. [[CrossRef](#)]
11. Kuo, H.-T.; Merckens, H.; Zhang, Z.; Uribe, C.F.; Lau, J.; Zhang, C.; Colpo, N.; Lin, K.-S.; Benard, F. Enhancing Treatment Efficacy of Lu-177-PSMA-617 with the Conjugation of an Albumin-Binding Motif: Preclinical Dosimetry and Endoradiotherapy Studies. *Mol. Pharm.* **2018**, *15*, 5183–5191. [[CrossRef](#)] [[PubMed](#)]
12. Kuo, H.-T.; Lin, K.-S.; Zhang, Z.; Uribe, C.F.; Merckens, H.; Zhang, C.; Bénard, F. <sup>177</sup>Lu-Labeled Albumin-Binder-Conjugated PSMA-Targeting Agents with Extremely High Tumor Uptake and Enhanced Tumor-to-Kidney Absorbed Dose Ratio. *J. Nucl. Med.* **2021**, *62*, 521–527. [[CrossRef](#)] [[PubMed](#)]
13. Wang, Z.; Tian, R.; Niu, G.; Ma, Y.; Lang, L.; Szajek, L.P.; Kiesewetter, D.O.; Jacobson, O.; Chen, X. Single Low-Dose Injection of Evans Blue Modified PSMA-617 Radioligand Therapy Eliminates Prostate-Specific Membrane Antigen Positive Tumors. *Bioconjug. Chem.* **2018**, *29*, 3213–3221. [[CrossRef](#)]
14. Zang, J.; Fan, X.; Wang, H.; Liu, Q.; Wang, J.; Li, H.; Li, F.; Jacobson, O.; Niu, G.; Zhu, Z.; et al. First-in-Human Study of <sup>177</sup>Lu-EB-PSMA-617 in Patients with Metastatic Castration-Resistant Prostate Cancer. *Eur. J. Nucl. Med. Mol. Imaging* **2019**, *46*, 148–158. [[CrossRef](#)] [[PubMed](#)]
15. Brandt, M.; Cardinale, J.; Giammei, C.; Guarrochena, X.; Hapfl, B.; Jouini, N.; Mindt, T.L. Mini-Review: Targeted Radiopharmaceuticals Incorporating Reversible, Low Molecular Weight Albumin Binders. *Nucl. Med. Biol.* **2019**, *70*, 46–52. [[CrossRef](#)] [[PubMed](#)]
16. van der Vusse, G.J. Albumin as Fatty Acid Transporter. *Drug Metab. Pharm.* **2009**, *24*, 300–307. [[CrossRef](#)] [[PubMed](#)]
17. Zorzi, A.; Middendorp, S.J.; Wilbs, J.; Deyle, K.; Heinis, C. Acylated Heptapeptide Binds Albumin with High Affinity and Application as Tag Furnishes Long-Acting Peptides. *Nat. Commun.* **2017**, *8*, 16092. [[CrossRef](#)]
18. Zorzi, A.; Linciano, S.; Angelini, A. Non-Covalent Albumin-Binding Ligands for Extending the Circulating Half-Life of Small Biotherapeutics. *MedChemComm* **2019**, *10*, 1068–1081. [[CrossRef](#)]
19. Zaman, R.; Islam, R.A.; Ibnat, N.; Othman, I.; Zaini, A.; Lee, C.Y.; Chowdhury, E.H. Current Strategies in Extending Half-Lives of Therapeutic Proteins. *J. Control Release* **2019**, *301*, 176–189. [[CrossRef](#)]
20. Zhang, P.; Xu, M.; Ding, J.; Chen, J.; Zhang, T.; Huo, L.; Liu, Z. Fatty Acid-Conjugated Radiopharmaceuticals for Fibroblast Activation Protein-Targeted Radiotherapy. *Eur. J. Nucl. Med. Mol. Imaging* **2021**, *49*, 1985–1996. [[CrossRef](#)]
21. Knudsen, L.B.; Lau, J. The Discovery and Development of Liraglutide and Semaglutide. *Front. Endocrinol.* **2019**, *10*, 155. [[CrossRef](#)] [[PubMed](#)]
22. Brooks, P.C.; Montgomery, A.M.P.; Rosenfeld, M.; Reisfeld, R.A.; Hu, T.; Klier, G.; Cheresch, D.A. Integrin Avβ3 Antagonists Promote Tumor Regression by Inducing Apoptosis of Angiogenic Blood Vessels. *Cell* **1994**, *79*, 1157–1164. [[CrossRef](#)]
23. Brooks, P.C.; Clark, R.A.F.; Cheresch, D.A. Requirement of Vascular Integrin Avβ3 for Angiogenesis. *Science* **1994**, *264*, 569–571. [[CrossRef](#)]
24. Shi, J.; Zhou, Y.; Chakraborty, S.; Kim, Y.-S.; Jia, B.; Wang, F.; Liu, S. Evaluation of <sup>111</sup>In-Labeled Cyclic RGD Peptides: Effects of Peptide and Linker Multiplicity on Their Tumor Uptake, Excretion Kinetics and Metabolic Stability. *Theranostics* **2011**, *1*, 322–340. [[CrossRef](#)] [[PubMed](#)]

25. Liu, S. Radiolabeled Cyclic RGD Peptide Bioconjugates as Radiotracers Targeting Multiple Integrins. *Bioconjug. Chem.* **2015**, *26*, 1413–1438. [[CrossRef](#)] [[PubMed](#)]
26. Gaertner, F.C.; Kessler, H.; Wester, H.-J.; Schwaiger, M.; Beer, A.J. Radiolabelled RGD Peptides for Imaging and Therapy. *Eur. J. Nucl. Med. Mol. Imaging* **2012**, *39* (Suppl. 1), S126–S138. [[CrossRef](#)] [[PubMed](#)]
27. Shi, J.; Wang, F.; Liu, S. Radiolabeled Cyclic RGD Peptides as Radiotracers for Tumor Imaging. *Biophys. Rep.* **2016**, *2*, 1–20. [[CrossRef](#)]
28. Ji, B.; Chen, B.; Wang, T.; Song, Y.; Chen, M.; Ji, T.; Wang, X.; Gao, S.; Ma, Q. <sup>99m</sup>Tc-3PRGD2 SPECT to Monitor Early Response to Neoadjuvant Chemotherapy in Stage II and III Breast Cancer. *Eur. J. Nucl. Med. Mol. Imaging* **2015**, *42*, 1362–1370. [[CrossRef](#)]
29. Zhu, Z.; Miao, W.; Li, Q.; Dai, H.; Ma, Q.; Wang, F.; Yang, A.; Jia, B.; Jing, X.; Liu, S.; et al. <sup>99m</sup>Tc-3PRGD2 for Integrin Receptor Imaging of Lung Cancer: A Multicenter Study. *J. Nucl. Med.* **2012**, *53*, 716–722. [[CrossRef](#)]
30. Jin, X.; Liang, N.; Wang, M.; Meng, Y.; Jia, B.; Shi, X.; Li, S.; Luo, J.; Luo, Y.; Cui, Q.; et al. Integrin Imaging with <sup>99m</sup>Tc-3PRGD2 SPECT/CT Shows High Specificity in the Diagnosis of Lymph Node Metastasis from Non-Small Cell Lung Cancer. *Radiology* **2016**, *281*, 958–966. [[CrossRef](#)]
31. Shi, J.; Fan, D.; Dong, C.; Liu, H.; Jia, B.; Zhao, H.; Jin, X.; Liu, Z.; Li, F.; Wang, F. Anti-Tumor Effect of Integrin Targeted <sup>177</sup>Lu-3PRGD2 and Combined Therapy with Endostar. *Theranostics* **2014**, *4*, 256–266. [[CrossRef](#)] [[PubMed](#)]
32. Gao, H.; Luo, C.; Yang, G.; Du, S.; Li, X.; Zhao, H.; Shi, J.; Wang, F. Improved in Vivo Targeting Capability and Pharmacokinetics of <sup>99m</sup>Tc-Labeled IsoDGR by Dimerization and Albumin-Binding for Glioma Imaging. *Bioconjug. Chem.* **2019**, *30*, 2038–2048. [[CrossRef](#)] [[PubMed](#)]
33. Nasrolahi Shirazi, A.; Oh, D.; Tiwari, R.K.; Sullivan, B.; Gupta, A.; Bothun, G.D.; Parang, K. Peptide Amphiphile Containing Arginine and Fatty Acyl Chains as Molecular Transporters. *Mol. Pharm.* **2013**, *10*, 4717–4727. [[CrossRef](#)] [[PubMed](#)]
34. Ehehalt, R.; Füllekrug, J.; Pohl, J.; Ring, A.; Herrmann, T.; Stremmel, W. Translocation of Long Chain Fatty Acids across the Plasma Membrane—Lipid Rafts and Fatty Acid Transport Proteins. *Mol. Cell. Biochem.* **2006**, *284*, 135–140. [[CrossRef](#)]
35. Munro, S. Lipid Rafts: Elusive or Illusive? *Cell* **2003**, *115*, 377–388. [[CrossRef](#)]
36. Shi, J.; Jin, Z.; Liu, X.; Fan, D.; Sun, Y.; Zhao, H.; Zhu, Z.; Liu, Z.; Jia, B.; Wang, F. PET Imaging of Neovascularization with <sup>68</sup>Ga-3PRGD2 for Assessing Tumor Early Response to Endostar Antiangiogenic Therapy. *Mol. Pharm.* **2014**, *11*, 3915–3922. [[CrossRef](#)]
37. Melemenidis, S.; Jefferson, A.; Ruparelia, N.; Akhtar, A.M.; Xie, J.; Allen, D.; Hamilton, A.; Larkin, J.R.; Perez-Balderas, F.; Smart, S.C.; et al. Molecular Magnetic Resonance Imaging of Angiogenesis In Vivo Using Polyvalent Cyclic RGD-Iron Oxide Microparticle Conjugates. *Theranostics* **2015**, *5*, 515–529. [[CrossRef](#)]
38. Chen, H.; Zhao, L.; Fu, K.; Lin, Q.; Wen, X.; Jacobson, O.; Sun, L.; Wu, H.; Zhang, X.; Guo, Z.; et al. Integrin Avβ3-Targeted Radionuclide Therapy Combined with Immune Checkpoint Blockade Immunotherapy Synergistically Enhances Anti-Tumor Efficacy. *Theranostics* **2019**, *9*, 7948–7960. [[CrossRef](#)]
39. Nieuwland, M.; Ruizendaal, L.; Brinkmann, A.; Kroon-Batenburg, L.; van Hest, J.C.M.; Löwik, D.W.P.M. A Structural Study of the Self-Assembly of a Palmitoyl Peptide Amphiphile. *Faraday Discuss.* **2013**, *166*, 360–379. [[CrossRef](#)]
40. Xu, F.; Chao, T.; Zhang, Y.; Hu, S.; Zhou, Y.; Xu, H.; Xiao, J.; Li, K. Chromosome 1 Sequence Analysis of C57BL/6J-Chr1<sup>KM</sup> Mouse Strain. *Int. J. Genom.* **2017**, *2017*, 1712530. [[CrossRef](#)]